NIH Public Access
Author Manuscript
Exp Neurol. Author manuscript; available in PMC 2016 January 01.

Published in final edited form as:
Exp Neurol. 2015 January ; 263: 190–199. doi:10.1016/j.expneurol.2014.10.005.

Axonal Charcot-Marie-Tooth Disease Patient-Derived Motor Neurons Demonstrate Disease-Specific Phenotypes including Abnormal Electrophysiological Properties

Mario A. Saporta, M.D. Ph.D[1,2], **Vu Dang, Ph.D.**[2], **Dmitri Volfson, Ph.D.**[2], **Bende Zou, M.D., Ph.D.**[3], **Xinmin (Simon) Xie, M.D., Ph.D.**[3], **Adijat Adebola, Ph.D.**[4], **Ronald K. Liem, Ph.D.**[4], **Michael Shy, M.D.**[1], and **John T. Dimos, Ph.D.**[2]

[1] Department of Neurology, University of Iowa

[2] iPierian Inc.

[3] AfaSci Inc.

[4] Department of Pathology and Cell Biology, Columbia University Medical Center

Abstract

Objective—Charcot-Marie-Tooth Disease (CMT) is a group of inherited peripheral neuropathies associated with mutations or copy number variations in over 70 genes encoding proteins with fundamental roles in the development and function of Schwann cells and peripheral axons. Here, we used iPSC-derived cells to identify common pathophysiological mechanisms in axonal CMT.

Methods—iPSC lines from patients with two distinct forms of axonal CMT (CMT2A and CMT2E) were differentiated into spinal cord motor neurons and used to study axonal structure and function and electrophysiological properties in vitro.

Results—iPSC-derived motor neurons exhibited gene and protein expression, ultrastructural and electrophysiological features of mature primary spinal cord motor neurons. Cytoskeletal abnormalities were found in neurons from a CMT2E (*NEFL*) patient and corroborated by a mouse model of the same *NEFL* point mutation. Abnormalities in mitochondrial trafficking were found in neurons derived from this patient, but were only mildly present in neurons from a CMT2A (*MFN2*) patient. Novel electrophysiological abnormalities, including reduced action potential threshold and abnormal channel current properties were observed in motor neurons derived from both of these patients.

Interpretation—Human iPSC-derived motor neurons from axonal CMT patients replicated key pathophysiological features observed in other models of MFN2 and NEFL mutations, including abnormal cytoskeletal and mitochondrial dynamics. Electrophysiological abnormalities found in

© 2014 Elsevier Inc. All rights reserved.

Corresponding author: Mario Saporta, M.D. Ph.D. Current address and Affiliation: Department of Neurology, Fluminense Federal University, Rua República do Peru 362/602, Rio de Janeiro RJ Brazil 22021-040, mariosaporta@gmail.com.

Publisher's Disclaimer: This is a PDF file of an unedited manuscript that has been accepted for publication. As a service to our customers we are providing this early version of the manuscript. The manuscript will undergo copyediting, typesetting, and review of the resulting proof before it is published in its final citable form. Please note that during the production process errors may be discovered which could affect the content, and all legal disclaimers that apply to the journal pertain.

NIH-PA Author Manuscript
NIH-PA Author Manuscript
NIH-PA Author Manuscript

NIH-PA Author Manuscript NIH-PA Author Manuscript NIH-PA Author Manuscript

axonal CMT iPSC-derived human motor neurons suggest that these cells are hyperexcitable and have altered sodium and calcium channel kinetics. These findings may provide a new therapeutic target for this group of heterogeneous inherited neuropathies.

Keywords

Axonal Charcot-Marie-Tooth Disease; Inherited Neuropathies; Motor Neurons; Induced Pluripotent Stem Cells; Axonal transport; electrophysiology

INTRODUCTION

Inherited neuropathies, collectively known as Charcot-Marie-Tooth disease (CMT), are the most common neurogenetic condition, affecting around 1 in every 2500 people worldwide (Nelis et al., 1996). Mutations in over 70 distinct genes have been associated with CMT, most of which affect proteins essential for Schwann cell and peripheral axon development and function (Saporta and Shy, 2013). Therefore, most CMT types can be classified by electrodiagnostic and pathological features as either demyelinating or axonal (Harding and Thomas, 1980). Demyelinating (type I) CMT is associated with mutations in genes encoding for myelin proteins (*PMP22*, *MPZ* and *CX32*) or transcription factors that regulate peripheral myelination (*EGR2*). Axonal (type II) CMT is frequently associated with mutations in proteins involved in maintaining axonal structure and function. For instance, mutations affecting cytoskeletal organization (*NEFL*, *HSPB1*) and axonal mitochondrial transport (*MFN2*) and function (*MFN2*, *GDAP1*) have all been linked to axonal forms of CMT. These genes seem to particularly impact peripheral axons from spinal cord motor and dorsal root ganglia neurons, hence causing peripheral neuropathies.

Despite significant advances in the biological understating of CMT, mostly derived from animal model and non-neuronal cell culture studies, there is still no effective treatment for any type of inherited neuropathy. Recent clinical trials investigating the therapeutic effect of ascorbic acid, previously demonstrated to improve the phenotype of a rodent model of a specific type of CMT (CMT1A) (Passage et al., 2004), failed to detect any significant clinical improvement in CMT1A patients ((Burns et al., 2009; Lewis et al., 2013; Micallef et al., 2009; Pareyson et al., 2011). The same is observed in other neurodegenerative and neurogenetic conditions, including amyotrophic lateral sclerosis and spinal muscular atrophy. This underscores the challenges in translating animal model findings into clinically relevant therapies for patients with neurological disorders and the need for new platforms that more closely reproduce the human disease. Current animal models used to study CMT, while extremely useful, differ considerably, from a genotypic standpoint, from patients, as significant genetic modifications have to be introduced to create a clinical phenotype that resembles the human disease.

The recent discovery of induced pluripotent stem cells (iPSC) (Takahashi and Yamanaka, 2006; Takahashi et al., 2007) combined with previous knowledge obtained from studies with human embryonic stem cells, established a new human platform for the study of neurogenetic conditions. Recent work in this field demonstrated that iPSC can be consistently obtained from healthy and affected individuals (Dimos et al., 2008) and

NIH-PA Author Manuscript

NIH-PA Author Manuscript

NIH-PA Author Manuscript

successfully differentiated into diverse central and peripheral nervous system cell types, including cholinergic spinal cord motor neurons, one of the main cell type affected by the inherited peripheral neuropathies (Saporta et al., 2011). Furthermore, disease specific phenotypes have been reported and, in some instances, corrected by pharmacological or genetic manipulations (Brennand et al., 2011; Ebert et al., 2009; Kazuki et al., 2010; Lee et al., 2009). This technology offers a unique opportunity to study human peripheral nervous system cell types affected by the inherited neuropathies, while maintaining the disease-associated genetic background of the patient.

In this study, we developed and characterized iPSC lines from 2 patients with early-onset, axonal forms of CMT caused by point mutations in *MNF2* and *NEFL* genes, differentiated these iPSC into spinal cord motor neurons and further expanded the phenotypic study of these motor neurons demonstrating specific abnormalities in mitochondrial dynamics, cytoskeletal organization and electrophysiological properties of these neuronal cells.

MATERIALS AND METHODS

Generation and characterization of human CMT iPSC

Fibroblast cultures were derived from skin punch biopsies of 2 patients with axonal forms of CMT and 3 unaffected control individuals, as part of an initiative to establish a CMT iPSC collection at the University of Iowa Neurology Department (described in Table 1). Fibroblasts were seeded on gelatin-coated 6-well plates and transduced with supernatant containing 4 retroviral vectors expressing *SOX2*, *OCT3/4*, *KFL4* and *C-MYC*. After 7 to 10 days, iPSC clones could be identified and selectively propagated on Matrigel (BD Bioscience, San Diego, CA)-coated plates in mTeSR1 (Stem Cell Technologies) defined media. A total of 3 to 6 iPSC clones per patient were expanded, banked and characterized. Pluripotency was established by gene expression profile (qPCR), immunostaining and spontaneous differentiation assays. The iPSC lines were also karyotyped and matched by DNA fingerprinting analyses to their parental fibroblast line (Cell Line Genetics, Madison, WI). To confirm the presence of the disease-causing mutation on each of the cell lines, direct sequencing was performed (GeneWiz, South Plainfield, NJ). All study participants gave written informed consent before enrollment. IRB approval was granted by the Wayne State University Human Investigation Committee.

Spinal cord motor neuron differentiation

iPSC were differentiated into spinal motor neurons as adherent cultures on Matrigel-coated culture plates using an established differentiation protocol based on dual SMAD inhibition (Burkhardt et al., 2013; Chambers et al., 2009). Briefly, colonies were expanded until 90 to 95% confluence was reached. Cells were then switched to knockout serum replacement medium containing 1 μM Dorsomorphine dihydrochloride (Tocris) and 10 μM SB431542 (Tocris) and after 3 days, gradually switched to N2 medium. On day 9, cultures were switched to a motor neuron maturation medium consisting of DMEM/F12 supplemented with B27, N2, 50mM ascorbic acid, 1.5 μM retinoic acid, 200 nM Smoothened Agonist (EMD Chemicals), 2 ng/mL BDNF, 2 ng/mL CTNF and 2 ng/mL GDNF and further matured for 9 days. Cultures were then dissociated and seeded on poly-L-lysine/laminin-

NIH-PA Author Manuscript NIH-PA Author Manuscript NIH-PA Author Manuscript

coated plates and cultured in motor neuron maturation medium until used in end-point experiments. For some experiments, neuronal cultures were magnetically sorted before end-point experiments (see below and in Fig. 1A).

Magnetic bead sorting of L1CAM (CD171)-positive neurons

Post-mitotic spinal cord motor neurons were enriched after dissociation at day 18 of the motor neuron differentiation protocol, by magnetic bead sorting. The primary antibody used was anti-L1CAM (CD171) (eBioscience, San Diego, CA) at a 1:20 dilution. Anti-PE microbeads, LS columns and a MidiMACS separator were used, following the manufacturer's protocols (Miltenyi Biotec GmbH, Bergisch Gladbach, Germany), available at https://www.miltenyibiotec.com.

Immunocytochemistry for neuronal development markers and cytoskeletal proteins

All primary antibodies used in this study are listed in Supplementary Table 1. Neuronal cultures were fixed in 4% paraformaldehyde for 20 min at room temperature, permeabilized with 0.2% Triton X-100 in 1x phosphate buffer saline (PBS) for 30 minutes and blocked with 10% donkey serum for 1 hour. Samples were incubated with the primary antibody solution overnight at 4°C. The following day, samples were washed four times with 0.01% Triton X-100 in 1x PBS and incubated with the secondary antibody solution for 1 hour. Samples were then counterstained with DAPI and examined under a Leica fluorescence or Nikon confocal microscope. For quantification of neurofilament content in neuronal cell bodies, cultures were double stained with TUJ1 and NEF-L antibodies and analyzed with Metaexpress software. Regions of interest (ROI) including TUJ1 and NEF-L immunoreactive areas of the cell body were marked and NEFL/TUJ1 ratios were calculated. For immunocytochemistry studies, two NEFL (CMT2E) and two MFN2 (CMT2A) clones were compared to three independent control lines.

RNA extraction and quantitative RT-PCR

Total cellular RNA was extracted from cell pellets using the RNeasy mini kit (QIAGEN, Valencia, CA), according to the manufacturer's instructions. Quantitative RT-PCR was performed using TaqMan RNA-to-Ct 1-Step Kit (Applied Biosystems, Carlsbad, CA, USA). TaqMan probes used in these experiments are described in Supplementary Table 2.

Time-lapse microscopy of axonal mitochondrial movement

Neuronal cultures were transfected at day 5 post-dissociation with *UBIQUITIN*-driven MitoDsRed and eGFP plasmids using FugeneHD (Roche) following the manufacturer's specifications. Briefly, 2 μl of each plasmid DNA was diluted in 100 μl of Opti-MEM (Invitrogen) and combined with 7 μl of the transfection reagent. The mixture was incubated for 15 minutes, diluted in 2.5 mL of motor neuron maturation media and added to cells. Media were changed the next day to remove the transfection reagent. Cultures were live-imaged at day 8 to 10 post-dissociation in a climate-controlled chamber (LiveCell, Pathology Devices, Westminster, MD, USA) at 37°C and 5% CO2, with a CCD camera mounted on a Nikon Eclipse Ti-U inverted fluorescence microscope, using NIS Elements software. Frames were acquired every 1 second for 5 minutes with a 40x objective. Axonal

NIH-PA Author Manuscript NIH-PA Author Manuscript NIH-PA Author Manuscript

mitochondrial movement was tracked and analyzed with custom-written Matlab routines. To determine that cells imaged were actually spinal cord motor neurons, plates were fixed immediately after live imaging and immunostained for ISLET1. Each individual live imaged-cell was retraced and ISLET1 immunoreactivity was confirmed. Mitochondria were classified according to previously established criteria (Baloh et al., 2007; Misko et al., 2010) as moving if they achieved a displacement greater than 2 μm. A velocity cutoff of 0.1 μm/s was used to define time spent paused. For time-lapse studies, data from three distinct MFN2 (CMT2A) clones, three NEFL (CMT2E) clones and two distinct controls were compared.

Electron microscopy of iPSC-derived neuronal cultures

Sample preparation and electron microscopy were performed at the Cell Sciences Imaging Facility – Stanford University following standard protocols. Briefly, neuronal cultures were plated in poly-L-lysine/laminin-coated 8-well culture slides (BD Biosciences, Franklin lakes, NJ, USA) and cultured for 10 days. Samples were fixed in 2 % Glutaraldehyde and 4% paraformaldehyde in 0.1M sodium cacodylate (pH ~7.2) for 20 minutes at room temperature and then moved to 4°C where they remained for at least 24 hours. The fixative solution was replaced with 1% OsO_4 in distilled water, gently rotated and left for 1 hr. After 3 brief washes with distilled water, samples were stained with 1% Uranyl acetate solution (in distilled water) overnight. Next, samples were dehydrated in a series of ethanol dilutions (50, 70, 95 and 100%) and acetonitrile and then embedded in epoxy resin. Tissue blocks were sectioned in 1 μm thickness and stained with methylene blue for light microscopic examination to locate areas of interest. Tissue blocks were then trimmed and sectioned into ultrathin sections for electron microscopy examination (Jeol TEM1230).

Electrophysiology

Whole-cell patch clamp recordings were performed on neurons that were co-cultured with primary human astrocytes for 10 – 21 days, after magnetic bead sorting (Lonza, Allendale, NJ, USA). The electrophysiologist was blinded to genotype when performing the experiments. Each set of experiments was repeated three times. The electrodes were pulled from borosilicate glass capillaries. In current-clamp recordings, cells were recorded in oxygenated external solution at room temperature, containing 119 mM NaCl, 2.5mM KCl, 1.3mM $MgSO_4$, 2.5 mM $CaCl_2$, 1 mM $Na2HPO_4$, 26.2 mM $NaHCO_3$, 11 mM glucose and perfused at a rate of 2 ml/min. The internal electrode solution for current clamp recordings consisted of: 120 mM potassium gluconate, 40 mM HEPES, 5 mM $MgCl_2$, 0.3 mM Mg-GTP, 2 mM Na-ATP, with pH adjusted to 7.2 with KOH. For voltage clamp recordings, the external solution consisted of 130 mM NaCl, 2 mM $MgCl_2$, 3mM KCl, 1 mM $CaCl_2$, 10 mM HEPES-Na, 10 mM Glucose. In voltage-clamp mode, for Na^+ current recordings, the internal solution consisted of 120 mM CsF, 10 mM HEPES, 11 mM EGTA, 1 mM $CaCl_2$, 1 mM $MgCl_2$, 10 mM TEA-Cl, 11 mM CsOH, and pH was adjusted to 7.4 using CsOH. For Ca^{2+} current recording, the external solution consisted of 115 mM Choline-Cl, 10 mM HEPES, 30 mM TEA-Cl, 10 mM Glucose, 2 mM $CaCl_2$, 0.5 μM TTX, pH was adjusted to 7.4 using HCl; the internal solution consisted of 125 mM CsCl, 1 mM $MgCl_2$, 2 mM $CaCl_2$, 10 mM EGTA, 10 mM HEPES, 4 mM MgATP and pH was adjusted to 7.4 using CsOH. For K^+ current recording, the internal solution consisted of 140 mM KCl, 10 mM HEPES, 2 mM $MgCl_2$, 11 mM EGTA, and 1.2 mM Mg-ATP. Tetrodotoxin (TTX 0.5 - 1 μM) was added to

NIH-PA Author Manuscript NIH-PA Author Manuscript NIH-PA Author Manuscript

the external solution to block Na^+ currents. For AHP recording, the internal solution consisted of 140 mM KCl, 10mM HEPES, 2 mM $MgCl_2$, 11 mM EGTA, and 1.2 mM Mg-ATP. The pH of all external and internal solutions was adjusted to 7.4 and 7.2, respectively. The osmolality of all solutions was adjusted to 280-300 mOsm/kg. The resistance of the pipette was approximately 2-3 (MΩ) in the bath solution. Following gigaohm seal, whole cell recording mode was established by breaking the membrane with rapid negative pressure and recordings were made using an Axo700B and DigiData 1440A A/D converter. The series resistance of pipettes was less than 10 MΩ and compensated for 70 - 80% using built in offset compensation circulatory of the Axon amplifier. Data were collected using pClamp V.10.2. Groups were composed of three distinct control lines and three clones each for the MFN2 (CMT2A) and NEFL (CMT2E) patients.

N98S *Nefl* Knockin Mice

Knock-in mice with the N98S *Nefl* mutation have been generated by Cre-LoxP homologous recombination (Adebola et al, unpublished observations). The mice are viable and fertile, but have a tremor. Spinal cords of 18-month old heterozygous mice (n = 3) were analyzed by immunohistochemistry using an anti-NEFL antibody and compared to wild type mice (n = 3). The animals are kept with IACUC approval (AC-AAAD6456) at Columbia University.

Statistical Analysis

Statistical analysis was performed using GraphPad Prism version 5.02 for Windows (GraphPad Software, San Diego, California USA). The Kruskal-Wallis test followed by Dunn's multiple comparison test was used to compare non-parametric variables from three different groups (MFN2/CMT2A, NEFL/CMT2E and control). Normally distributed data were analyzed with univariate ANOVA followed by Tukey's multiple comparison test. For two-group comparison, Mann–Whitney U-test was performed for non-parametric variables and unpaired t-test for parametric variables. A *p*-value of < 0.05 was considered significant. Significance levels were marked on figures as follows: $*p < 0.05$, $** p < 0.01$, $***p < 0.001$. Morphometric, molecular and electrophysiological studies were carried out in a completely blinded fashion.

RESULTS

Induced pluripotent stem cell lines generated from patients with axonal forms of Charcot-Marie-Tooth disease

Skin fibroblasts from 2 patients with axonal CMT and three non-affected controls were transduced with retroviral vectors expressing 4 transcription factors (*OCT4*, *SOX2*, *KLF4*, and *CMYC*). Demographic and clinical information for each of these patients, the control individuals, as well as other patients included in the CMT iPSC collection at the University of Iowa, are summarized in Table 1. Four weeks after viral transduction, ES-like colonies were selected for further expansion (Suppl. Fig. 1A). At least 3 clones from each patient's iPSC were developed. All of these iPSC lines exhibited characteristic hESC morphology (Suppl. Fig. 1B), were able to form embryoid bodies (Suppl. Fig. 1C) and be differentiated in cell types from all three embryonic germ layers following a spontaneous differentiation protocol (Suppl. Fig. 1D, E and F), confirming their pluripotency *in vitro.* These cells also

NIH-PA Author Manuscript

NIH-PA Author Manuscript

NIH-PA Author Manuscript

expressed pluripotency markers including NANOG, SSEA3 and TRA1-60 (Suppl. Fig. 1G and H). Quantitative RT-PCR revealed that endogenous pluripotency-associated genes, including *NANOG*, *CDH1*, *LIN28*, *NODAL*, *FOXD3* and *TDGF1* were expressed at higher levels in the iPSCs when compared to the originating fibroblast lines, and at similar levels to established hESC lines (Suppl. Fig. 2). The presence of the respective disease-causing mutation could be confirmed by direct sequencing in all cell lines derived from the CMT2A ($MFN2_{R364W/+}$) and CMT2E ($NEFL_{N98S/+}$) patients (Suppl. Fig. 1). Cell lines from all CMT patients and controls had normal karyotypes (Suppl. Fig. 1J and K).

Spinal cord motor neuron differentiation from CMT human iPSC

CMT iPSC were differentiated into spinal cord motor neurons as adherent cultures with neuralization by dual SMAD signaling inhibition and patterning with retinoic acid and activation of Sonic Hedgehog pathway, as previously reported (Burkhardt et al., 2013; Chambers et al., 2009) (Fig. 1A). Starting at day 25 post-differentiation, mature cells expressing neuronal cytoskeletal proteins, including neurofilament light chain (Fig. 1B-D) and the motor neuron transcription factors ISLET1 (Fig. 1B), LHX3 (Fig. 1C) and HB9 (Fig. 1D) could be observed, confirming their ventral spinal cord identity. To increase the percentages of mature motor neurons and decrease the percentages of neural progenitors in culture, magnetic bead based enrichment for L1CAM, a neuronal cell adhesion molecule associated with axon guidance and cell migration, was used at day 18 post-differentiation. Gene expression analysis by qPCR demonstrated enrichment of markers associated with motor neuron identity, including *ISLET1*, *HB9* (*MNX1*) and *NFM* and depletion of markers associated with neural progenitors, including *PAX6* and *OLIG2* (Suppl. Fig. 3) after magnetic sorting. L1CAM-enriched neurons were electrically active when co-cultured with human astrocytes for 14 to 21 days (Fig. 1E-H), as previously described (Johnson et al., 2007). IPSC-derived motor neurons exhibit TTX sensitive evoked (Fig. 1E) and spontaneous bursts of action potentials (Fig. 1F), and excitatory and inhibitory postsynaptic potentials could also be detected at hyperpolarized holding membrane potentials between ¯60 and ¯70 mV (Fig. 1G-H), similar to what is commonly observed in primary neurons in culture. Ultrastructural imaging of these neuronal cultures identified specific structures, including microtubule and neurofilament-rich perikarya (Fig. 1I) and axons (Fig. 1J), and synaptic terminals containing synaptic vesicles (Fig. 1J). Mitochondria were present along axons and typically concentrated in the axonal hillock and synaptic terminal regions of the cells (Fig. 1I and J).

Characterization of disease-specific phenotypes in iPSC-derived motor neurons from patients with axonal (type II) CMT

Axonal (type II) CMT is caused by mutations in genes regulating the structure and function of peripheral axons, specifically those of spinal cord motor neurons and dorsal root ganglia sensory neurons. In order to investigate the ability of iPSC-derived neurons to model CMT, we focused our phenotypic studies in cell lines derived from two patients with early-onset, axonal forms of CMT, CMT2E (NEFL) (Mersiyanova et al., 2000) and CMT2A (MFN2) (Züchner et al., 2004).

NIH-PA Author Manuscript NIH-PA Author Manuscript NIH-PA Author Manuscript

Abnormal neurofilament accumulation in the cell body of *NEFL*-mutant, iPSC-derived human spinal cord motor neurons

Mutations in the neurofilament light gene (*NEFL*) cause CMT2E, an autosomal dominant form of axonal inherited neuropathy. Previous work has demonstrated that most *NEFL* mutations interfere with the normal assembly of the intermediate filament network, usually leading to defects in the assembly and transport of NEF-L (Gentil et al., 2012; Perez-Olle et al., 2004; Pérez-Ollé et al., 2005). Wild type NEF-L is normally distributed throughout the cell body and processes of transfected neuronal cell lines, while CMT2E pathogenic NEF-L mutants usually accumulate in the neuronal cell body and disrupt axonal mitochondrial transport (Gentil et al., 2012; Pérez-Ollé et al., 2005). In order to study the cytoskeletal organization of iPSC-derived human CMT motor neurons, immunostaining for all major intermediate filaments (including NEF-L, NEF-M, NEF-H, internexin and peripherin) and for βIII-tubulin was performed in neuronal cultures at day 28 of differentiation from two clones from the NEFL (CMT2E) and MFN2 (CMT2A) patients and also from two distinct controls and imaged in a confocal microscope. A subgroup of spinal cord motor neurons characterized by a strong immunoreactivity to neurofilament antibodies in their neuronal cell body could be easily identified in iPSC-derived motor neuron cultures from all three groups (Fig. 2 A1-A4), suggesting a more mature spinal cord motor neuron identity, according to the co-expression of ISLET1 (Fig. 2B), and choline acetyltransferase (ChAT) (Suppl. Fig. 4 A - D). In this specific subpopulation of motor neurons, an increased accumulation of NEFL was observed in the perikarya of neurons derived from two distinct clones from the CMT2E ($NEFL_{N98S/+}$) patient when compared to two controls and two MFN2-mutant neuronal lines, representing two distinct clones from the CMT2A patient (Fig. 2 A1-A4). This was further quantified by calculating the ratio of NEFL immunoreactivity over βIII tubulin (TUJ1) reactivity in their neuronal cell bodies, to account for differences in neuronal cell body size. A significant increase in this ratio was observed in both NEFL-mutant clones ($p < 0.001$), and to a lesser degree, in one of the MFN2 clones ($p < 0.01$), when compared to the control cell lines (Fig. 2C). Interestingly, the same pattern of NEFL accumulation in the perikarya of spinal cord motor neurons was observed in a knock-in mouse model of the same NEFL N98S mutation (Fig. 2D and E). These mice present a similar clinical phenotype to the CMT2E patient recruited for this study, including axonal peripheral neuropathy and hearing loss and also demonstrated NEFL accumulation in the cell body of neurons in the cerebellum and brain stem (Adebola et al, unpublished observations). This abnormal accumulation was not observed in the wild type mice. Ultrastructural analysis of NEFL neuronal cultures derived from the CMT2E patient did not uncover any abnormal aggregation of intermediate filaments in either the neuronal cell body or the neuronal processes (Suppl. Fig. 4E and F) of these cells. This absence of aggregates may suggest that the abnormal accumulation of neurofilament proteins in the cell body of the NEFL mutant cells is likely due to abnormal trafficking of the protein leaving the soma and moving along the axon, rather than being related to an amyloidogenic property of the mutant protein. This is further supported by ultrastructural analysis of NEFL N98S knockin mice sciatic nerves, which uncovered significant reduction of neurofilaments in the axons of these animals, in the absence of clear aggregation formation (Suppl. Fig. 4G and H).

NIH-PA Author Manuscript NIH-PA Author Manuscript NIH-PA Author Manuscript

Impaired mitochondrial transport in iPSC-derived axonal CMT human spinal cord motor neurons

Abnormal axonal mitochondrial trafficking has been implicated in the pathogenesis of several forms of axonal CMT. Axonal mitochondria spend more time paused and undergo slower anterograde and retrograde movements in murine neurons expressing *Mfn2* disease mutants and this effect is independent from MFN2's role in mitochondrial fusion (Baloh et al., 2007; Misko et al., 2010), suggesting that abnormal mitochondrial trafficking may be part of the pathophysiology of CMT2A. Clustering of mitochondria was previously observed in cell bodies and proximal axons of rat DRG neurons expressing CMT2E–associated mutant NEFL proteins (Pérez-Ollé et al., 2005). Recently, similar changes in axonal mitochondrial transport have been described in a mouse model of another axonal form of CMT (CMT2F) caused by mutation in the *Hspb1* gene (d'Ydewalle et al., 2011). In order to study axonal mitochondrial kinetics in our human CMT neuronal cells, control, MFN2-mutant and NEFL-mutant iPSC-derived neuronal cultures were transfected with plasmids coding for *UBIQUITIN*-driven eGFP and MitoDsRed at day 20 of differentiation and live imaged under controlled conditions (Figure 3A-C, respectively) at day 28 of differentiation. At least 10 neurons were imaged per condition (disease clone or control). To confirm their spinal motor neuron identity, cells were fixed and stained for ISLET1 immediately after live microscopy and imaged under a confocal microscope (Figure 3 D1-D4). Mitochondrial kinetics was quantified by automated, unbiased image processing. Number and size of mitochondria did not differ between two control lines and lines from a MFN2 (CMT2A) and NEFL (CMT2E) patient (two clones each) (Figures 3E and F). Quantification of percentages of moving mitochondria along axons did not suggest any significant difference between the three groups either (Figure 3G). However, CMT2E mitochondria travelled shorter distances (Figure 3H) at slower velocities (Figure 3I and J) when compared to control mitochondria, suggesting that the mutant NEFL protein affected the ability of mitochondria to traffic along axons. Of note, a trend towards shorter displacement was also observed in MFN2 mitochondrial kinetics when compared to control, but did not reach statistical significance ($p > 0.05$). Nonetheless, MFN2-mutant mitochondria moved at slower anterograde and retrograde velocities when compared to control mitochondria ($p < 0.01$). These changes were of a significantly lower magnitude than those described in studies using rodent primary neurons (Baloh et al., 2007; Misko et al., 2010).

Altered electrophysiological properties of CMT iPSC-derived motor neurons

Spinal motor neuron hyperexcitability has been observed in mouse models of SOD1 familial amyotrophic lateral sclerosis (Kuo et al., 2004; Zona et al., 2006) and hypothesized to be a possible mechanism for neuronal and axonal degeneration. Recently, an iPSC-based study on the pathophysiology of distinct forms of familial ALS (including *SOD1*, *FUS* and *C9orf72*) has suggested a common feature of intrinsic membrane hyperexcitability in motor neurons from all these distinct genetic etiologies (Wainger et al., 2014). Spinal motor neuron hyperexcitability has also been described after neonatal axotomy and deemed to occur, at least in part, due to loss of trophic factors derived from muscles (Mentis et al., 2007). In order to explore the possibility that the early changes in axonal physiology present in axonal

NIH-PA Author Manuscript NIH-PA Author Manuscript NIH-PA Author Manuscript

CMT could be associated with similar abnormalities in neuronal excitability, electrophysiological recordings were made from iPSC-derived spinal motor neurons from controls, MFN2 (CMT2A) and NEFL (CMT2E) patients (Fig. 4A). Assessment of action potential threshold shows that MNF2 and NEFL motor neurons fire action potentials at significantly more hyperpolarized membrane potentials when compared to control neurons (⁻45.2 +/− 1 mV, ⁻43.8 +/− 1 mV and ⁻39.4 +/− 1 mV respectively, p <0.001) (Fig. 4B), suggesting that they are in a hyperexcitable state. In order to better characterize this phenomenon, experiments were performed to study sodium channel kinetics. MFN2 motor neurons had higher sodium current densities when compared to control and NEFL lines (Fig. 4C and D). Furthermore, despite showing identical activation curves when compared to control motor neurons (not depicted), MFN2 motor neurons demonstrated a reduced degree of channel inactivation (Fig. 4E), not seen in NEFL motor neurons (Fig. 4F). Sodium channels from CMT2A motor neurons also recovered more rapidly from inactivation when compared to matched controls. Assessment of voltage dependent calcium channel (VDCC) function demonstrated slightly lower channel densities in NEFL motor neurons (Fig. 4G) with the activation curve shifted towards more polarized (positive) membrane potentials ($V_{1/2}$ = ⁻14 +/− 5 mV) compared to control and MFN2 lines ($V_{1/2}$ = _21 +/− 3 and ⁻24 mV respectively, $p < 0.05$). Interestingly, a use-dependent protocol applied to determine channel inactivation revealed that VDCCs from NEFL and MFN2 motor neurons demonstrate less inactivation than VDCCs from control motor neurons (Fig. 4H). Taken together, these results suggest that axonal CMT motor neurons are hyperexcitable and demonstrate changes in sodium and calcium channel dynamics, which may be related to this increased excitability and could be a target for therapeutical intervention.

DISCUSSION

In this study, we created a new resource for the study of inherited neuropathies by generating iPSC and neuronal cell cultures from patients with various forms of Charcot-Marie-Tooth disease (CMT). We demonstrated that spinal cord motor neurons generated from patients with early-onset, axonal forms of CMT present discrete abnormalities in axonal mitochondrial transport that may play a role in the pathogenesis of these diseases. We also demonstrated that human NEFL mutant (CMT2E) motor neurons accumulate intermediate filaments in their cell body in vitro, similarly to spinal cord motor neurons of heterozygous mice expressing the same NEFL point mutation. Lastly, we identified altered electrophysiological properties in spinal motor neurons derived from patients with axonal CMT that can contribute to neuronal hyperexcitability. These results support the use of iPSC-derived models as a human platform to study inherited neuropathies.

Inherited neuropathies as a group are the most common neurogenetic condition, affecting approximately 125,000 people in the US alone and causing significant disability and quality of life impairment. From a biological standpoint, inherited neuropathies offer a naturally occurring model to study peripheral nervous system function and pathophysiology, as they are associated with mutations in genes that play important roles in Schwann cell and axonal physiology (Saporta and Shy, 2013). Despite the significant advances in our understanding of the biology of inherited neuropathies, there are no specific treatments currently available for patients. Cellular reprogramming offers an alternative, scalable source of human spinal

NIH-PA Author Manuscript

NIH-PA Author Manuscript

NIH-PA Author Manuscript

cord motor neurons and glia cells carrying the same genetic background of patients with inherited neuropathies for use in translational and drug discovery studies, and requires only minimally invasive techniques such as skin biopsy or blood draws for their development.

Our study demonstrates that human iPSC-derived motor neurons can recapitulate key disease-related features previously uncovered in animal and cell-based models of axonal CMT, including abnormal mitochondrial trafficking and cytoskeletal distribution in a system that more closely recapitulates the genetic mechanisms associated with patient pathophysiology. For instance, most disease models of autosomal dominant axonal CMT are based on knock out rodents or cell systems where only either the wild type or the mutant protein is expressed, whereas patients with these types of axonal CMT are heterozygotes for the genetic mutation, therefore carrying a normal copy of the gene. This may explain the milder phenotypes found in our neurons when compared to studies where knock out mice or cell systems have been used, especially in the case of MFN2. *Mfn2* knockout cells have significant impairment of mitochondrial axonal transport, as do cells expressing only disease-related mutant MFN2 (Baloh et al., 2007; Misko et al., 2010, 2012). Our results suggest that, when present in heterozygosis, *MFN2* mutations do not cause severe impairment in mitochondrial fusion or trafficking along axons, at least not as severe as suggested by previous models. This is of particular importance when considering translating findings from these models to clinical research and practice, as some of the phenotypes found in animal model studies are not biologically similar to the phenotypes found in patients. It also raises the question as to what is the mechanism behind MFN2 associated axonal degeneration in patients with CMT2A, a line of investigation that could uncover novel targets for CMT treatment.

Our findings from the *NEFL* mutant neuronal cultures closely resemble previous reports from cell culture studies (Perez-Olle et al., 2004; Pérez-Ollé et al., 2005) and, more recently, a mouse model of the same point mutation (Adebola and Liem, unpublished observations). Both human and mouse heterozygous N98S *NEFL* neurons show increased neurofilament accumulation in their perikarya and significantly impaired mitochondrial movement along their axons. These similar findings between two different models with the identical genetic abnormality (heterozygous N98S point mutation in *NEFL*) provide stronger evidence of its role in the pathophysiology of CMT2E and confirm that, for some specific forms of axonal CMT, impaired mitochondrial trafficking is part of the disease mechanism.

To our knowledge, this is the first work to systematically study electrophysiological properties of human axonal CMT spinal cord motor neurons. Our findings indicate that motor neurons from CMT2A and CMT2E patients are hyperexcitable, as they generate action potentials at lower membrane potential thresholds compared to control neurons. Moreover, we found abnormalities in ion channel physiology that may be related to this hyperexcitable state. MFN2-mutant motor neurons had an increased density of sodium currents in their membrane, and their voltage-dependent sodium channels demonstrated impaired inactivation after a use-dependent paradigm, compared to controls. Although NEFL-mutant motor neurons did not demonstrate the altered sodium channel function as MFN2-mutant neurons, they have decreased VDCCs density as well as an activation curve that is shifted towards more polarized membrane potentials. Both MFN2-mutant and NEFL-

NIH-PA Author Manuscript NIH-PA Author Manuscript NIH-PA Author Manuscript

mutant motor neurons showed impaired inactivation of VDCCs as well. Whether these changes in neuronal excitability and ion channel function are cause or consequence of the axonal degeneration associated with these forms of CMT remains to be determined. Interestingly, ion channel dysfunction has been recently associated with several forms of peripheral neuropathies, including a specific type of axonal CMT (CMT2C), which was associated to point mutations in TRPV4, a member of the TRP family of cationic channels (Landouré et al., 2010); and idiopathic small fiber neuropathy, associated with mutation in the sodium channel Na(v)1.7 in up to 28% of cases (Han et al., 2012). There is growing evidence that increased neuronal firing may lead to axonal degeneration, possibly due to Na^+/K^+ pump failure and Ca^{2+} influx, and this may be a common downstream mechanism for most of the axonal peripheral neuropathies. Therefore, these new findings suggest a novel therapeutic target for axonal CMT. Modulating ion channel activity and reducing neuronal hyperexcitability may be protective to the neuron and prevent or reduce axonal degeneration associated with CMT. A recent study using primary rat dorsal ganglia neurons (Misko et al., 2012) demonstrated that Tetrodotoxin (TTX), a sodium channel blocker, was able to reduce axonal degeneration in neurons expressing disease-associated *mfn2* mutations, a result consistent with our findings. The use of targeted less toxic sodium channel blockers may prove helpful in reducing axonal degeneration in patients with CMT2A, and may be the foundation for a novel clinical intervention strategy.

Neuronal lines from the two axonal CMT patients showed somewhat differing phenotypes, as expected, considering that they are related to two different genetic mechanisms (NEFL mutations in CMT2E and MFN2 mutations in CMT2A). Therefore, it is expected that the basic pathophysiology of these two conditions will differ; however, our data suggest that downstream mechanisms (abnormal axonal mitochondrial movement and neuronal hyperexcitability) may play a role in both conditions and may be an opportunity for common therapeutic interventions in the future.

In summary, our results demonstrate that iPSC-derived motor neurons are a feasible new platform for the study of inherited neuropathies and that further studies focusing in common downstream events in the pathophysiology of axonal CMT forms may provide novel common therapies for this group of inherited peripheral neuropathies.

Supplementary Material

Refer to Web version on PubMed Central for supplementary material.

ACKNOWLEDGEMENTS

M.A.S. was funded by a fellowship from the RDCRN Inherited Peripheral Neuropathy Consortium, National Institutes of Health. This work was supported by NINDS/Office of Rare Diseases grant 5U54NS065712 (M.E.S.) and NIH grants R01MH078194, R43NS065555, and R43 NS073311 (X.S.X) and RC1 NS068131 (RKL). This study was also supported by resources from iPierian Inc. The authors would like to thank Mary Reilly, Jun Li, Peter Bingham and Richard Finkel and their respective teams for providing patients' samples and clinical information. The authors would also like to thank the research team from iPierian Inc for technical assistance during this study, including Fernando Martinez, Rita Martinez, Uzma Shoukat-Mumtaz, Hui Gai, Allen Reed, Eileen Rose, Jeff Garnes and Brian Christie.

NIH-PA Author Manuscript NIH-PA Author Manuscript NIH-PA Author Manuscript

REFERENCES

Baloh RH, Schmidt RE, Pestronk A, Milbrandt J. Altered axonal mitochondrial transport in the pathogenesis of Charcot-Marie-Tooth disease from mitofusin 2 mutations. J. Neurosci. 2007; 27:422–30. doi:10.1523/JNEUROSCI.4798-06.2007. [PubMed: 17215403]

Brennand KJ, Simone A, Jou J, Gelboin-Burkhart C, Tran N, Sangar S, Li Y, Mu Y, Chen G, Yu D, McCarthy S, Sebat J, Gage FH. Modelling schizophrenia using human induced pluripotent stem cells. Nature. 2011; 473:221–5. doi:10.1038/nature09915. [PubMed: 21490598]

Burkhardt MF, Martinez FJ, Wright S, Ramos C, Volfson D, Mason M, Garnes J, Dang V, Lievers J, Shoukat-Mumtaz U, Martinez R, Gai H, Blake R, Vaisberg E, Grskovic M, Johnson C, Irion S, Bright J, Cooper B, Nguyen L, Griswold-Prenner I, Javaherian A. A cellular model for sporadic ALS using patient-derived induced pluripotent stem cells. Mol. Cell. Neurosci. 2013; 56:355–64. doi:10.1016/j.mcn.2013.07.007. [PubMed: 23891805]

Burns J, Ouvrier RA, Yiu EM, Joseph PD, Kornberg AJ, Fahey MC, Ryan MM. Ascorbic acid for Charcot-Marie-Tooth disease type 1A in children: a randomised, double-blind, placebo-controlled, safety and efficacy trial. Lancet Neurol. 2009; 8:537–44. doi:10.1016/S1474-4422(09)70108-5. [PubMed: 19427269]

Chambers SM, Fasano CA, Papapetrou EP, Tomishima M, Sadelain M, Studer L. Highly efficient neural conversion of human ES and iPS cells by dual inhibition of SMAD signaling. Nat. Biotechnol. 2009; 27:275–80. doi:10.1038/nbt.1529. [PubMed: 19252484]

d'Ydewalle C, Krishnan J, Chiheb DM, Van Damme P, Irobi J, Kozikowski AP, Vanden Berghe P, Timmerman V, Robberecht W, Van Den Bosch L. HDAC6 inhibitors reverse axonal loss in a mouse model of mutant HSPB1-induced Charcot-Marie-Tooth disease. Nat. Med. 2011; 17:968–74. doi:10.1038/nm.2396. [PubMed: 21785432]

Dimos JT, Rodolfa KT, Niakan KK, Weisenthal LM, Mitsumoto H, Chung W, Croft GF, Saphier G, Leibel R, Goland R, Wichterle H, Henderson CE, Eggan K. Induced pluripotent stem cells generated from patients with ALS can be differentiated into motor neurons. Science. 2008; 321:1218–21. doi:10.1126/science.1158799. [PubMed: 18669821]

Ebert AD, Yu J, Rose FF, Mattis VB, Lorson CL, Thomson JA, Svendsen CN. Induced pluripotent stem cells from a spinal muscular atrophy patient. Nature. 2009; 457:277–80. doi:10.1038/nature07677. [PubMed: 19098894]

Gentil BJ, Minotti S, Beange M, Baloh RH, Julien J-P, Durham HD. Normal role of the low-molecular-weight neurofilament protein in mitochondrial dynamics and disruption in Charcot-Marie-Tooth disease. FASEB J. 2012; 26:1194–203. doi:10.1096/fj.11-196345. [PubMed: 22155564]

Han C, Hoeijmakers JGJ, Ahn H-S, Zhao P, Shah P, Lauria G, Gerrits MM, te Morsche RHM, Dib-Hajj SD, Drenth JPH, Faber CG, Merkies ISJ, Waxman SG. Nav1.7-related small fiber neuropathy: impaired slow-inactivation and DRG neuron hyperexcitability. Neurology. 2012; 78:1635–43. doi:10.1212/WNL.0b013e3182574f12. [PubMed: 22539570]

Harding AE, Thomas PK. The clinical features of hereditary motor and sensory neuropathy types I and II. Brain. 1980; 103:259–80. [PubMed: 7397478]

Johnson MA, Weick JP, Pearce RA, Zhang S-C. Functional neural development from human embryonic stem cells: accelerated synaptic activity via astrocyte coculture. J. Neurosci. 2007; 27:3069–77. doi:10.1523/JNEUROSCI.4562-06.2007. [PubMed: 17376968]

Kazuki Y, Hiratsuka M, Takiguchi M, Osaki M, Kajitani N, Hoshiya H, Hiramatsu K, Yoshino T, Kazuki K, Ishihara C, Takehara S, Higaki K, Nakagawa M, Takahashi K, Yamanaka S, Oshimura M. Complete genetic correction of ips cells from Duchenne muscular dystrophy. Mol. Ther. 2010; 18:386–93. doi:10.1038/mt.2009.274. [PubMed: 19997091]

Kuo JJ, Schonewille M, Siddique T, Schults ANA, Fu R, Bär PR, Anelli R, Heckman CJ, Kroese ABA. Hyperexcitability of cultured spinal motoneurons from presymptomatic ALS mice. J. Neurophysiol. 2004; 91:571–5. doi:10.1152/jn.00665.2003. [PubMed: 14523070]

Landouré G, Zdebik AA, Martinez TL, Burnett BG, Stanescu HC, Inada H, Shi Y, Taye AA, Kong L, Munns CH, Choo SS, Phelps CB, Paudel R, Houlden H, Ludlow CL, Caterina MJ, Gaudet R, Kleta R, Fischbeck KH, Sumner CJ. Mutations in TRPV4 cause Charcot-Marie-Tooth disease type 2C. Nat. Genet. 2010; 42:170–4. doi:10.1038/ng.512. [PubMed: 20037586]

NIH-PA Author Manuscript NIH-PA Author Manuscript NIH-PA Author Manuscript

Lee G, Papapetrou EP, Kim H, Chambers SM, Tomishima MJ, Fasano CA, Ganat YM, Menon J, Shimizu F, Viale A, Tabar V, Sadelain M, Studer L. Modelling pathogenesis and treatment of familial dysautonomia using patient-specific iPSCs. Nature. 2009; 461:402–6. doi:10.1038/nature08320. [PubMed: 19693009]

Lewis, R. a; McDermott, MP.; Herrmann, DN.; Hoke, A.; Clawson, LL.; Siskind, C.; Feely, SME.; Miller, LJ.; Barohn, RJ.; Smith, P.; Luebbe, E.; Wu, X.; Shy, ME. High-dosage ascorbic acid treatment in Charcot-Marie-Tooth disease type 1A: results of a randomized, double-masked, controlled trial. JAMA Neurol. 2013; 70:981–7. doi:10.1001/jamaneurol.2013.3178. [PubMed: 23797954]

Mentis GZ, Díaz E, Moran LB, Navarrete R. Early alterations in the electrophysiological properties of rat spinal motoneurones following neonatal axotomy. J. Physiol. 2007; 582:1141–61. doi:10.1113/jphysiol.2007.133488. [PubMed: 17510183]

Mersiyanova IV, Perepelov AV, Polyakov AV, Sitnikov VF, Dadali EL, Oparin RB, Petrin AN, Evgrafov OV. A new variant of Charcot-Marie-Tooth disease type 2 is probably the result of a mutation in the neurofilament-light gene. Am. J. Hum. Genet. 2000; 67:37–46. doi:10.1086/302962. [PubMed: 10841809]

Micallef J, Attarian S, Dubourg O, Gonnaud P-M, Hogrel J-Y, Stojkovic T, Bernard R, Jouve E, Pitel S, Vacherot F, Remec J-F, Jomir L, Azabou E, Al-Moussawi M, Lefebvre M-N, Attolini L, Yaici S, Tanesse D, Fontes M, Pouget J, Blin O. Effect of ascorbic acid in patients with Charcot-Marie-Tooth disease type 1A: a multicentre, randomised, double-blind, placebo-controlled trial. Lancet Neurol. 2009; 8:1103–10. doi:10.1016/S1474-4422(09)70260-1. [PubMed: 19818690]

Misko A, Jiang S, Wegorzewska I, Milbrandt J, Baloh RH. Mitofusin 2 is necessary for transport of axonal mitochondria and interacts with the Miro/Milton complex. J. Neurosci. 2010; 30:4232–40. doi:10.1523/JNEUROSCI.6248-09.2010. [PubMed: 20335458]

Misko AL, Sasaki Y, Tuck E, Milbrandt J, Baloh RH. Mitofusin2 mutations disrupt axonal mitochondrial positioning and promote axon degeneration. J. Neurosci. 2012; 32:4145–55. doi:10.1523/JNEUROSCI.6338-11.2012. [PubMed: 22442078]

Nelis E, Van Broeckhoven C, De Jonghe P, Löfgren A, Vandenberghe A, Latour P, Le Guern E, Brice A, Mostacciuolo ML, Schiavon F, Palau F, Bort S, Upadhyaya M, Rocchi M, Archidiacono N, Mandich P, Bellone E, Silander K, Savontaus ML, Navon R, Goldberg-Stern H, Estivill X, Volpini V, Friedl W, Gal A. Estimation of the mutation frequencies in Charcot-Marie-Tooth disease type 1 and hereditary neuropathy with liability to pressure palsies: a European collaborative study. Eur. J. Hum. Genet. 1996; 4:25–33. [PubMed: 8800924]

Pareyson D, Reilly MM, Schenone A, Fabrizi GM, Cavallaro T, Santoro L, Vita G, Quattrone A, Padua L, Gemignani F, Visioli F, Laurà M, Radice D, Calabrese D, Hughes RAC, Solari A. Ascorbic acid in Charcot-Marie-Tooth disease type 1A (CMT-TRIAAL and CMT-TRAUK): a double-blind randomised trial. Lancet Neurol. 2011; 10:320–8. doi:10.1016/S1474-4422(11)70025-4. [PubMed: 21393063]

Passage E, Norreel JC, Noack-Fraissignes P, Sanguedolce V, Pizant J, Thirion X, Robaglia-Schlupp A, Pellissier JF, Fontés M. Ascorbic acid treatment corrects the phenotype of a mouse model of Charcot-Marie-Tooth disease. Nat. Med. 2004; 10:396–401. doi:10.1038/nm1023. [PubMed: 15034573]

Perez-Olle R, Jones ST, Liem RKH. Phenotypic analysis of neurofilament light gene mutations linked to Charcot-Marie-Tooth disease in cell culture models. Hum. Mol. Genet. 2004; 13:2207–20. doi:10.1093/hmg/ddh236. [PubMed: 15282209]

Pérez-Ollé R, López-Toledano MA, Goryunov D, Cabrera-Poch N, Stefanis L, Brown K, Liem RKH. Mutations in the neurofilament light gene linked to Charcot-Marie-Tooth disease cause defects in transport. J. Neurochem. 2005; 93:861–74. doi:10.1111/j.1471-4159.2005.03095.x. [PubMed: 15857389]

Saporta MA, Grskovic M, Dimos JT. Induced pluripotent stem cells in the study of neurological diseases. Stem Cell Res. Ther. 2011; 2:37. doi:10.1186/scrt78. [PubMed: 21936964]

Saporta MA, Shy ME. Inherited peripheral neuropathies. Neurol. Clin. 2013; 31:597–619. doi:10.1016/j.ncl.2013.01.009. [PubMed: 23642725]

NIH-PA Author Manuscript

NIH-PA Author Manuscript

NIH-PA Author Manuscript

Takahashi K, Tanabe K, Ohnuki M, Narita M, Ichisaka T, Tomoda K, Yamanaka S. Induction of pluripotent stem cells from adult human fibroblasts by defined factors. Cell. 2007; 131:861–72. doi:10.1016/j.cell.2007.11.019. [PubMed: 18035408]

Takahashi K, Yamanaka S. Induction of pluripotent stem cells from mouse embryonic and adult fibroblast cultures by defined factors. Cell. 2006; 126:663–76. doi:10.1016/j.cell.2006.07.024. [PubMed: 16904174]

Wainger BJ, Kiskinis E, Mellin C, Wiskow O, Han SSW, Sandoe J, Perez NP, Williams LA, Lee S, Boulting G, Berry JD, Brown RH, Cudkowicz ME, Bean BP, Eggan K, Woolf CJ. Intrinsic membrane hyperexcitability of amyotrophic lateral sclerosis patient-derived motor neurons. Cell Rep. 2014; 7:1–11. doi:10.1016/j.celrep.2014.03.019. [PubMed: 24703839]

Zona C, Pieri M, Carunchio I. Voltage-dependent sodium channels in spinal cord motor neurons display rapid recovery from fast inactivation in a mouse model of amyotrophic lateral sclerosis. J. Neurophysiol. 2006; 96:3314–22. doi:10.1152/jn.00566.2006. [PubMed: 16899637]

Züchner S, Mersiyanova IV, Muglia M, Bissar-Tadmouri N, Rochelle J, Dadali EL, Zappia M, Nelis E, Patitucci A, Senderek J, Parman Y, Evgrafov O, Jonghe P, De, Takahashi Y, Tsuji S, Pericak-Vance MA, Quattrone A, Battaloglu E, Polyakov AV, Timmerman V, Schröder JM, Vance JM, Battologlu E. Mutations in the mitochondrial GTPase mitofusin 2 cause Charcot-Marie-Tooth neuropathy type 2A. Nat. Genet. 2004; 36:449–51. doi:10.1038/ng1341. [PubMed: 15064763]

NIH-PA Author Manuscript

NIH-PA Author Manuscript

NIH-PA Author Manuscript

Highlights

- Patient –derived spinal motor neurons closely resemble primary neurons;
- CMT2E neurons have disrupted neurofilament and axonal mitochondrial dynamics;
- CMT2A and CMT2E neurons are hyperexcitable and have altered ion channel kinetics;
- Therefore, our results suggest a novel potential target for drug therapy in CMT.
- Our data supports the use of cellular reprogramming to study Inherited Neuropathies

NIH-PA Author Manuscript

NIH-PA Author Manuscript

NIH-PA Author Manuscript

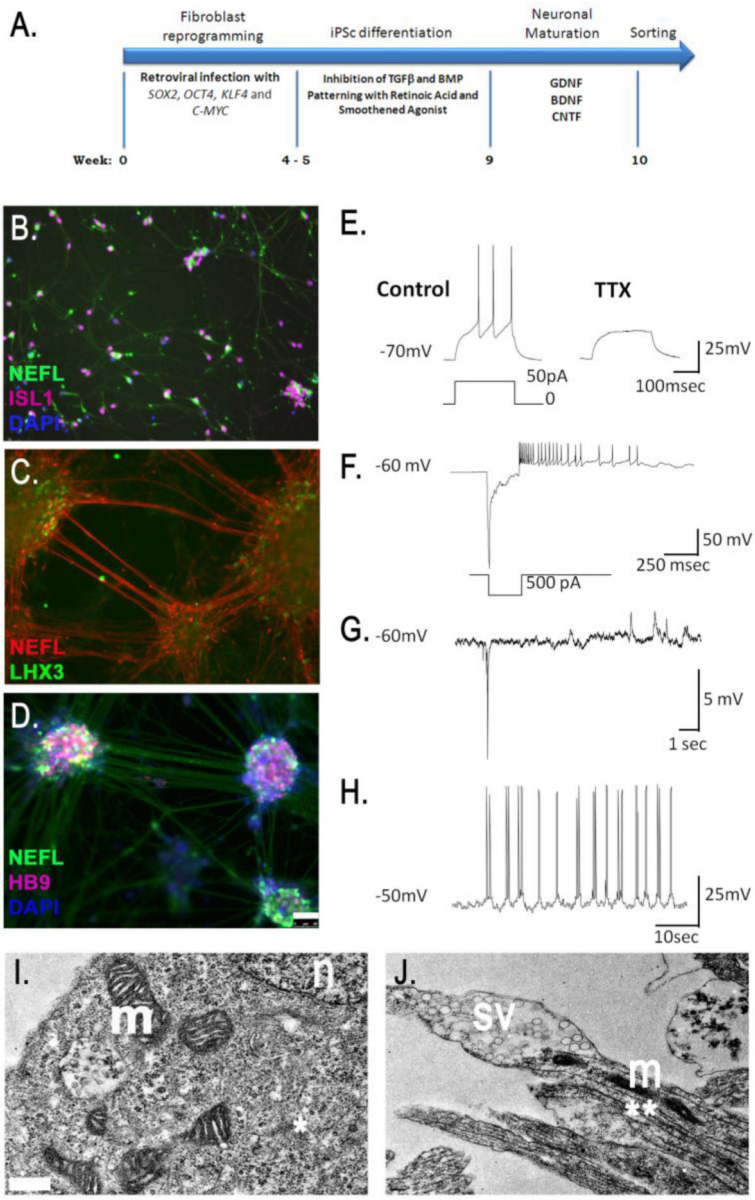

Figure 1. Motor neuron differentiation and characterization

Spinal cord motor neurons were generated from iPSC of patients with CMT and unaffected controls following a dual SMAD inhibition protocol modified from reference (16) (A). Twenty days after dissociation of the neuronal cultures, expression of the neuronal cytoskeletal protein NEFL and the transcription factor ISL1 could be observed (in this example, after magnetic bead sorting of neuronal cultures at dissociation (day 18) using L1CAM antibodies) (B.) After long-term culture (over 45 days), expression of the medial motor column marker LHX3 (C) and the somatic motor neuron transcription factor HB9 (D) could be observed in most of the neurons. Note that at this time point, spinal cord motor neurons tend to cluster (scale bar for B – D = 50 μm). Current clamp recordings of iPSC generated MNs demonstrate TTX sensitive action potentials elicited by depolarizing current step (E) and I_h current elicited by hyperpolarizing current step (F). Spontaneous IPSPs and

NIH-PA Author Manuscript

NIH-PA Author Manuscript

NIH-PA Author Manuscript

EPSCs (G) and spontaneous bursts of action potentials (H) could also be identified in these cultures. Taken together, these data demonstrate that iPSC derived motor neurons have similar electrophysiological properties as mature primary neurons. Ultrastructural imaging of the neuronal cultures revealed cells with typical neuronal features including the presence of cytoskeletal proteins (* = neurofilament and ** = microtubules) and mitochondria (m) concentrated in the axon hillock (I) and pre-synaptic vesicles (sv) at the axon terminal (J). n = nucleus (Scale bar for I and J = 0.5 μm).

NIH-PA Author Manuscript

NIH-PA Author Manuscript

NIH-PA Author Manuscript

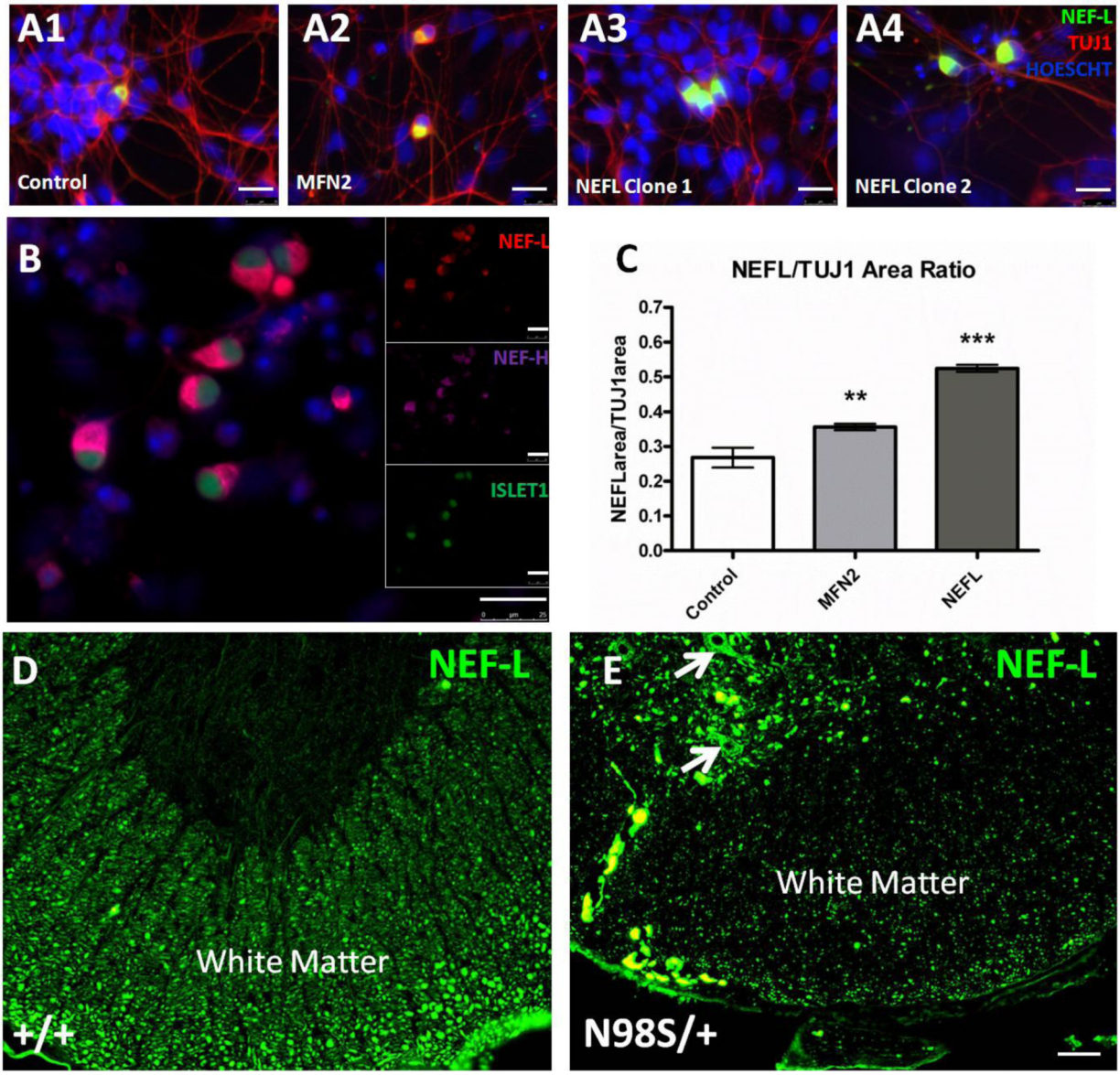

Figure 2. Increased neurofilament accumulation in the perikarya of NEFL (CMT2E) motor neurons

Immunocytochemistry for TUJ1 and NEF-L revealed a significant increase of NEF-L accumulation in the cell body of NEFL motor neurons (A3 and A4), when compared to control (A1) and MFN2 (A2) motor neurons. The ventral motor neuron identity of these cells was confirmed by triple staining with NEF-L, NEF-H and ISLET1 (B). To further characterize this phenotype, automated quantification of the relative area of NEFL staining was performed, by calculating the ratio of NEFL over TUJ1 staining. This quantification revealed a significant increase in the relative area of NEF-L staining in the NEFL neurons, when compared to MFN2 and control neurons (** $p < 0.01$, *** $p < 0.001$) (F). Immunostaining for NEFL in the ventral horn of spinal cords from wild type (G) and knock-in N98S/+ (H) mice revealed the same increase in NEF-L immunoreactivity in the perikarya of N98S/+ neurons (arrows). Note the reduced NEFL staining in the whiter matter tracts of

the N98S/+ mouse, suggesting impaired trafficking of NEF-L to the axons of spinal cord motor neurons. Scale bar for A1-A4, B, D and E: 25 μm.

NIH-PA Author Manuscript
NIH-PA Author Manuscript
NIH-PA Author Manuscript

NIH-PA Author Manuscript

NIH-PA Author Manuscript

NIH-PA Author Manuscript

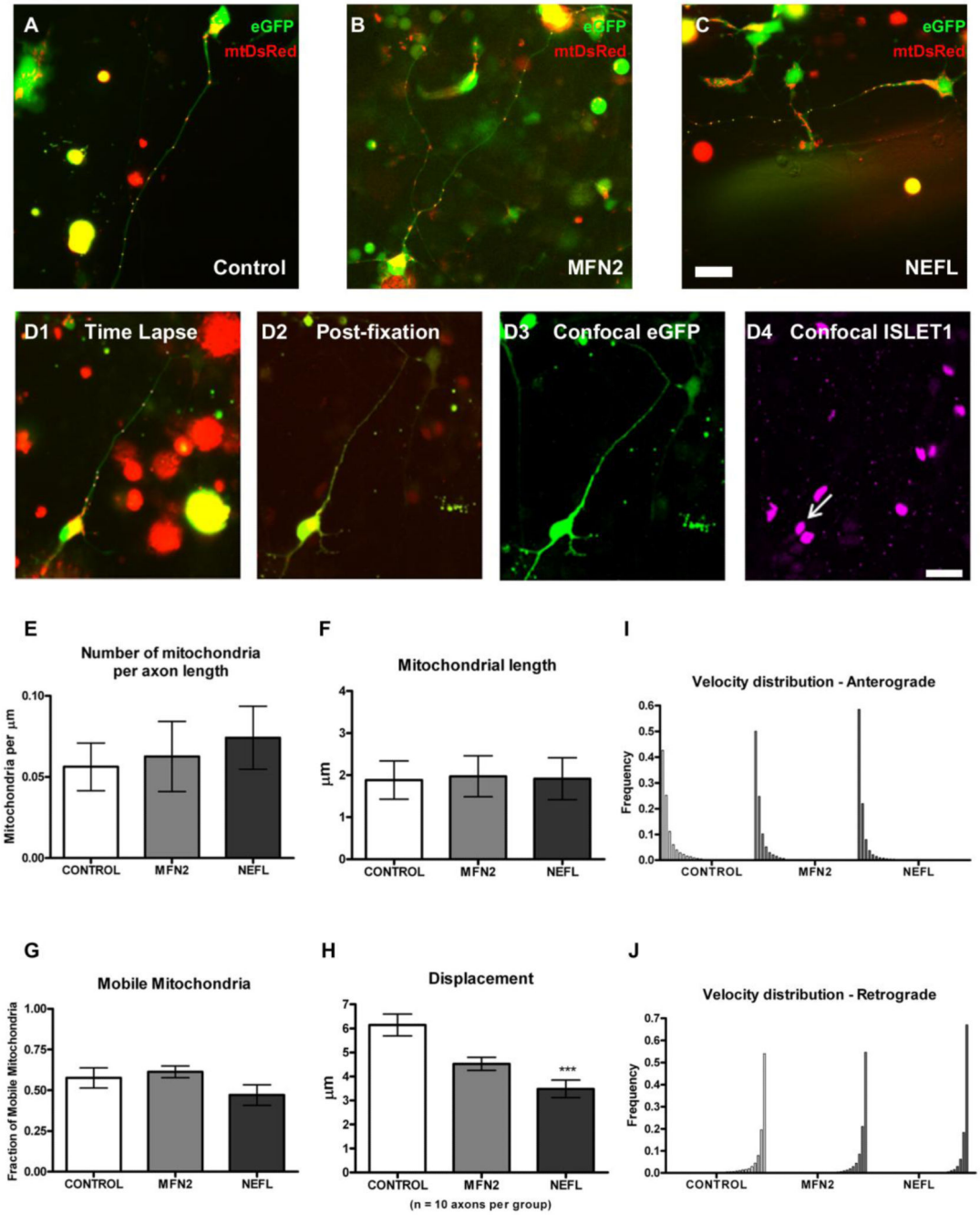

Figure 3. Abnormal mitochondrial trafficking in axons of patient-derived NEFL (CMT2E) and MFN2 (CMT2A) motor neurons

Neuronal cultures from control (A), MFN2 (B) and NEFL (C) individuals were transfected with *UBIQUITIN*-driven constructs coding for eGFP and MitoDsRed. Individual neurons (at least 10 per genotype) were imaged by time-lapse microscopy and their coordinates recorded (D1). Next, cultures were fixed and stained for ISLET1 and neurons were retraced (D2) and imaged by confocal microscopy to confirm co-localization of eGFP (D3) and ISLET1 (D4). Mitochondrial morphology and kinetics were determined using custom-written Matlab routines. No significant differences in mitochondrial numbers (E) or length

NIH-PA Author Manuscript

NIH-PA Author Manuscript

NIH-PA Author Manuscript

(F) between groups were observed. There was a trend towards reduced mitochondrial mobility in NEFL motor neurons (G) ($p > 0.05$) and mobile mitochondria in this group also had significantly reduced displacement (H) (*** $p < 0.001$). There was only a trend for smaller displacement in MFN2 mitochondria, compared to controls ($p > 0.05$). A significant reduction in both mitochondrial anterograde (I) and retrograde (J) velocities was also observed in the NEFL motor neurons and, to a lesser degree, in MFN2 motor neurons ($p < 0.01$). Scale bar for A – C: 25 μm; for D1 – D4: 25 μm.

NIH-PA Author Manuscript

NIH-PA Author Manuscript

NIH-PA Author Manuscript

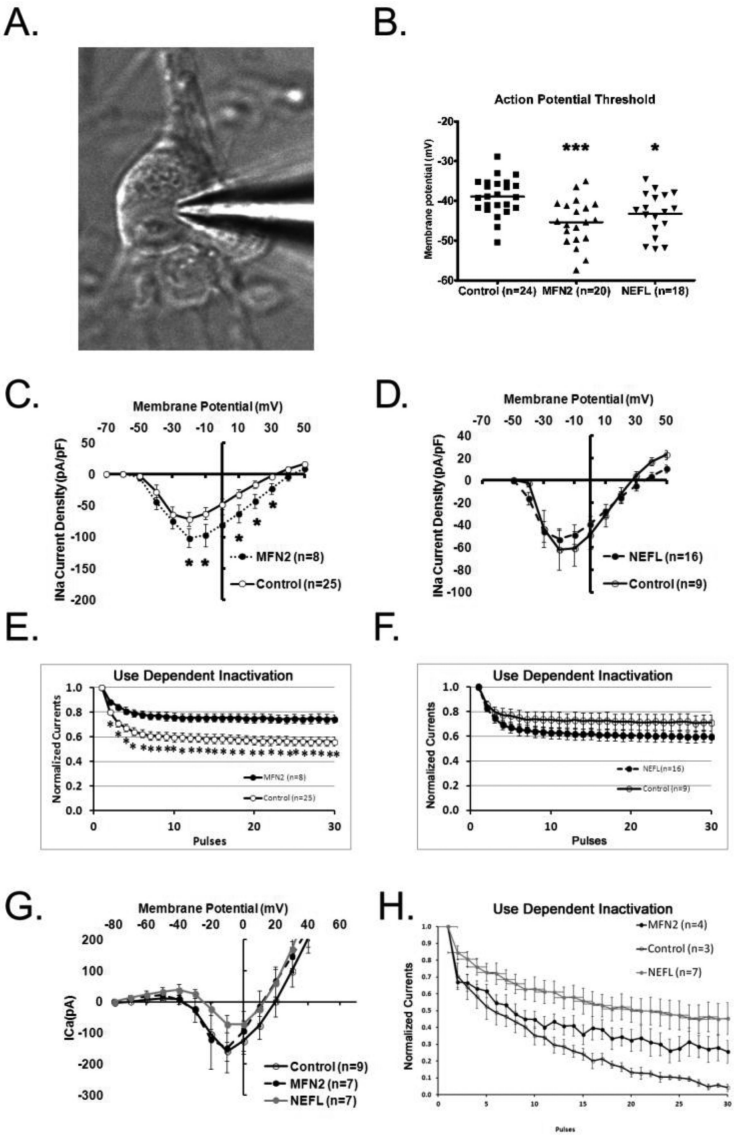

Figure 4. Changes in sodium and calcium channel dynamics and neuronal hyperexcitability in axonal CMT motor neurons

Electrophysiological recordings were made from spinal motor neurons derived from controls, MFN2 and NEFL patients (A). Assessment of action potential threshold shows that MFN2 and NEFL motor neurons fire action potentials at significantly more hyperpolarized membrane potentials when compared to control neurons (* $p < 0.05$, ***$^{-}p < 0.001$) (B). Current voltage chart showing current densities for control and MFN2 (C) and control and NEFL (D) motor neurons uncovered higher sodium current densities in MFN2 neurons. Use dependent inactivation curves for sodium currents for control and MNF2 (E) and control and NEFL (F) motor neurons also demonstrate changes in the MFN2 (CMT2A) neurons, with sodium channels inactivating less than in controls and NEFL (CMT2E) neurons. Current voltage chart showing current densities for control, NEFL and MFN2 motor neurons demonstrated slightly reduced calcium channel density in NEFL (CMT2E) motor neurons (G). Use dependent inactivation curves for calcium currents for control, MFN2 and NEFL

motor neurons uncovered reduced inactivation of calcium channels in both MFN2 and NEFL motor neurons.

NIH-PA Author Manuscript
NIH-PA Author Manuscript
NIH-PA Author Manuscript

NIH-PA Author Manuscript

NIH-PA Author Manuscript

NIH-PA Author Manuscript

Table 1

Charcot-Marie-Tooth iPSC collection at the University of Iowa.

Sample	CMT type	Age (years)	Gender	CMTNS	Gene	Mutation
Patient 1	**CMT 2A**	**42**	**M**	**33**	**MFN2**	**c.1090C>T (R364W)**
Patient 2	**CMT 2E**	**12**	**F**	**7**	**NEFL**	**c.293A>G (N98S)**
Patient 3	CMT1B	30	F	9	MPZ	c.116A>C (H39P)
Patient 4	CMT 4A	5	M	8	GDAP1	c.577A>T (L193X) c.1019ins (R341Fs)
Patient 5	CMT1A	53	F	11	PMP22	PMP22 duplication
Patient 6	CMT1A	60	M	23	PMP22	PMP22 duplication
Patient 7	CMT1A	61	F	23	PMP22	PMP22 duplication
Patient 8	CMT1A	57	M	24	PMP22	PMP22 duplication
Patient 9	CMT1X	47	F	3	GJB1	c.193T>C (Y65H)
Patient 10	CMT1X	19	M	22	GJB1	c.193T>C (Y65H)
Patient 11	CMT 4J	46	F	MND	FIG4	c.122T>C (I41T) c.718C>T (R183X)
Patient 12	CMT 4J	44	M	MND	FIG4	c.122T>C (I41T) c.718C>T (R183X)
Control 1	**NA**	**10**	**M**	**NA**	**NA**	**NA**
Control 2	**NA**	**29**	**F**	**NA**	**NA**	**NA**
Control 3	**NA**	**86**	**F**	**NA**	**NA**	**NA**

MND: Motor neuron disease phenotype. NA: Not applicable.

In bold: cell lines used in this study